The bloodstream form of *Trypanosoma brucei* displays non-canonical gluconeogenesis

Julie Kovářová[1,*], Martin Moos[2], Michael P. Barrett[3], David Horn[4], Alena Zíková[1]

[1] Institute of Parasitology, Biology Centre of the Czech Academy of Sciences, České Budějovice, Czech Republic

[2] Institute of Entomology, Biology Centre of the Czech Academy of Sciences, České Budějovice, Czech Republic

[3] Wellcome Centre for Integrative Parasitology, University of Glasgow, Glasgow, United Kingdom

[4] Wellcome Centre for Anti-Infectives Research, University of Dundee, Dundee, United Kingdom

* Corresponding author: julie.kovarova@paru.cas.cz

Abstract

Trypanosoma brucei is the causative agent of the Human and Animal African Trypanosomiases. Mammalian stage parasites infect the bloodstream, central nervous system, but also skin, adipose tissue or lungs. They rely on ATP produced in glycolysis, consuming large amounts of glucose which is readily available in mammalian tissues. In addition to glucose, glycerol can be utilised as a carbon and ATP source and also as a substrate for gluconeogenesis. The physiological relevance of glycerol-fed gluconeogenesis for mammalian-infective trypanosome life-cycle stages, however, remins elusive. Loss of the canonical gluconeogenic enzyme, fructose-1,6-bisphosphatase, does not abolish the process hence at least one other enzyme must participate in gluconeogenesis in trypanosomes. Using a combination of CRISPR/Cas9 gene editing and RNA interference, we generated mutants for four enzymes potentially capable of contributing to gluconeogenesis: fructose-1,6-bisphoshatase, sedoheptulose-1,7-bisphosphatase, phosphofructokinase, transaldolase, alone or in various combinations. Metabolomic analyses revealed that flux through gluconeogenesis was maintained irrespective of which of these genes were lost. Our data renders unlikely a previously hypothesised role of a reverse phosphofructokinase reaction in gluconeogenesis and precludes the participation of a novel biochemical pathway involving transaldolase in the process. Sustained metabolic flux in gluconeogenesis in our mutants, including in a triple-null strain, provides new insights into gluconeogenesis and the pentose phosphate pathway, and

improves the current understanding of carbon metabolism of the mammalian-infective stages of *T. brucei*.

Introduction

Trypanosoma brucei brucei is the causative agent of Human African Trypanosomiasis, also termed sleeping sickness [1]. The mammalian infective stage of the parasite is called the bloodstream form (BSF), and it is transmitted between hosts by blood-feeding tsetse flies. In the first stage of the disease, these extracellular parasites divide in the bloodstream of the mammalian host. If left untreated, the trypanosomes invade the central nervous system, manifesting as the second stage of the disease. Bloodstream form parasites can also inhabit skin, adipose tissue, lungs and other tissues [1-5]. Previous dogma stated that BSF trypanosomes are absolutely glucose-dependent, however, we [6] and others [7] have shown that they also employ gluconeogenesis and can use glycerol as a carbon source. It is still unclear whether the adipose tissue forms use glycerol via gluconeogenesis as an energy source, largely due to technical challenges associated with such studies. However, it has become clear that the parasite's metabolism is highly flexible and adaptable, which should be considered when developing drugs against metabolic targets, and it is notable that adipose tissue forms are less responsive to several trypanocidal drugs [8].

Glycolysis is indispensable to BSF trypanosomes, has a very high flux and is the major producer of ATP under standard culture conditions [9]. Gluconeogenesis (GNG) is a metabolic pathway that produces sugars from non-sugar carbon sources. In the case of BSF *T. brucei*, the GNG pathway includes conversion of glycerol into glucose 6-phosphate (G6P). GNG primarily uses the same enzymes as glycolysis, but operating in the opposite direction. The key difference between the two pathways is the step between fructose 6-phosphate (F6P), and fructose 1,6-bisphosphate (F1,6bP) when phosphofructokinase (PFK) phosphorylates F6P in glycolysis, while fructose-1,6-bisphosphatase (FBPase) dephosphorylates fructose 1,6-bisphosphate (F1,6bP) to form fructose 6-phosphate (F6P) [10]. In addition, when glycerol is used as a substrate, glycerol kinase (GK) becomes a key enzyme of GNG [7].

Previously, we demonstrated the presence of GNG in the BSF by silencing the glucose transporters by RNAi knockdown [6]. The observed lethal phenotype was rescued by the addition of glycerol to the culture media. As verified by targeted LC-MS metabolomics, glycerol was incorporated into fructose 6-phosphate (F6P) and other metabolites via GNG. The same conclusion was reached by Pineda and colleagues after adapting BSF parasites to glucose-free glycerol-containing medium [7]. Surprisingly, however, GNG was not abolished after deletion of the *FBPase* gene indicating an involvement of another, so far unknown, enzyme [6, 7].

GNG and FBPase was also studied in the insect procyclic form (PCF) of *T. brucei* [11]. This stage has a more elaborate mitochondrion in terms of both morphology and metabolism, which can provide additional substrates for GNG. Hence, proline is utilised by PCF as a carbon source, via proline degradation in the mitochondrion, and fed into GNG via phosphoenolpyruvate carboxykinase or pyruvate phosphate dikinase [11]. FBPase knock-out (KO) PCF cells are viable when grown in the absence of glucose, although these cells do display a mild growth defect, and defects in metacyclogenesis and transmission through the tsetse fly. The activity of FBPase can be compensated by another unknown enzyme, since GNG from proline still takes place following FBPase KO [11]. Glycerol is the preferred carbon source over glucose in PCF trypanosomes, since glycerol kinase has approximately 80-times higher activity than hexokinase [12].

In the majority of eukaryotic cells studied to date, the balance between FBPase and PFK activity is very strictly and tightly regulated [10]. FBPase is positively regulated by ATP, and negatively by AMP and fructose 2,6-bisphosphate (F2,6bP). PFK is controlled by the same metabolites in a reciprocal manner, i. e positively by AMP, ADP, and F2,6P. The mechanism, which has been described in detail, guarantees mutual exclusivity of these two reactions, and prevents futile cycling (a situation when both reactions would be running in a cycle, only consuming ATP). However, this fine control appears to be missing from *T. brucei*, since PFK is much less sensitive to inhibition by ATP, and not affected by F2,6bP (see below, [13]). F2,6bP is an activator of most eukaryotic PFK enzymes, normally produced from F1,6bP by the bifunctional enzyme, 6-phosphofructo-2-kinase/fructose-2,6-bisphosphatase,but this enzymatic activity is uncertain in *T. brucei*. Four homologous proteins were found to be encoded in the genome of *T. brucei*, and all of them were predicted to localise to the cytosol [14]. However, based on the recent Tryptag project, at least one of them (PFK-2/FBPase-2 Tb1,

Tb927.8.1020) seems to localise to glycosomes, where glycolysis takes place [15], and PFK-2 activity was measured for this protein [14]. Regulation of *T. brucei* FBPase has not been reported so far.

Although PFK from *T. brucei* is an ATP-dependent enzyme, its amino acid sequence is a 'chimera' between the pyrophosphate- and ATP-dependent enzymes [16]. When PFK was isolated from *T. brucei*, and its sensitivity to potential regulatory molecules tested, AMP was found to be the only allosteric activator, although 10-times less potent than for the leishmania enzyme [13, 16]. Phosphoenolpyruvate acted as an allosteric inhibitor, whereas F1,6bP or F2,6bP did not significantly influence enzyme activity [13]. As predicted by a model, and experimentally validated, PFK is in excess in *T. brucei* and glycolytic flux is reduced only after depletion of PFK beyond 60 % of WT activity. Depletion of PFK reduced glycolytic flux to 26 %, although it is unclear whether the effect is direct, or a secondary consequence of decreased activity of other glycolytic enzymes (hexokinase, enolase, pyruvate kinase) [9]. Highly specific allosteric inhibitors of *T. brucei* PFK have been developed, and shown to be effective in killing BSF parasites *in vitro* and in infected mice [17]. Fernandes [18] reported reversed activity of PFK *in vitro*, but the physiological relevance of this observation is unclear as reversed activity of three mammalian PFK isoforms that had been measured *in vitro* is thought to be absent *in vivo* [19].

In trypanosomatids, both glycolytic and gluconeogenic enzymes are localised within specialized organelles called glycosomes. Glycosomes are highly adapted peroxisomes, and they share related PEX-dependent import machineries [20]. In trypanosomatids, these organelles also harbour parts of the pentose phosphate pathway (PPP), nucleotide metabolism, and other associated pathways. The arrangement and function of the PPP is not fully resolved in *T.brucei* BSF because transketolase is not expressed in this stage, but transaldolase is, resulting in an incomplete non-oxidative branch of the PPP (Fig 1A) [21, 22]. The glycosomal membrane is 'semi-permeable', and thought to allow free passage of small molecules (up to 6 carbons based on a mathematical model) through open channels, but impermeable to larger molecules [23, 24]. Hence, cofactors such as ADP/ATP or NAD^+/NADH are balanced inside glycosomes, and glycosomal localisation of the glycolytic enzymes has important implications for their regulation [25].

We and others have shown previously that deletion of the *FBPase* gene does not eliminate the enzymatic activity responsible for dephosphorylation of F1,6bP (Kovarova, Pineda), indicating that other enzymes capable of this activity are also present. Notably, a gene encoding sedoheptulose-1,7-bisphosphatase (SBPase), an enzyme typically involved in the Calvin cycle of plants, is present in the genome of *T. brucei*. Due to a relatively high sequence identity (26 %) to FBPase, we considered it a possible candidate for possessing FBPase activity. Hence, we created a double knock-out cell line, for FBPase and SBPase (*Δfbp.sbp*). We also explored two other scenarios where PFK [18] or a pathway involving transaldolase (Hannaert) could bypass FBPase in GNG, although neither hypothesis was retained. The enzyme(s) responsible for GNG flux remain a mystery, but we present several metabolomic datasets that provide new insights into GNG and PPP in bloodstream trypanosomes.

Materials and Methods

T. brucei cell culture and cell line construction

Bloodstream form *Trypanosoma brucei brucei* Lister 427 cells were cultured in HMI-11 medium [26] supplemented with 10 % FCS (BioSera) at 37°C and 5 % CO_2. The fructose-1,6-bisphosphatase and sedoheptulose-1,7-bisphosphatase knock-out cell line (*Δfbp.sbp*) was generated by CRISPR/Cas9 gene editing in the $2T1^{T7\text{-}Cas9}$ cell line [27]. In order to delete *FBP* (Tb927.9.8720), a template for sgRNA transcription was synthesised by end-filling PCR with primers FBPgRNA_F and sgRNA_R, and a repair template for DNA integration was synthesised with primers FBP.NPT50_5 and FBP.NPT50_3. Cas9 expression was induced with tetracycline at 1 µg/ml (InvivoGen) 24 h prior to transfection with Amaxa nucleofector (Lonza) using programme Z-001. First, the *Δfbp* cell line was generated, and after validation of successful replacement of both *FBP* alleles with a G418 resistance cassette, a subsequent transfection was performed to replace the *SBP* (Tb927.2.5800) alleles with a puromycin resistance cassette (primer pairs SBPgRNA_F and sgRNA_R for sgRNA, and SBP.PAC50_5 and SBP.PAC50_3 for the repair template with puromycin resistance). Likewise, Δ*tal* (TAL is encoded by Tb927.8.5600) was generated in the parental and *Δfbp.sbp* cell lines, using primer pairs AZ1550 and sgRNA_R for sgRNA, and AZ1551 and AZ1552 for the repair template with phleomycin resistance. The primers used are listed in Table 1. Hygromycin was used at 5 µg/ml (InvivoGen), blasticidin at 5 µg/ml (InvivoGen), G418 at 2.5 µg/ml (Invivogen), and puromycin at 0.1 µg/ml (InvivoGen).

For depletion of PFK (Tb927.3.3270), the RNAi plasmid p2T7-177 [28] was used, digested with BamHI and HindIII. A *PFK* PCR product was amplified using primer pair AZ1339 and AZ1340, digested with the same restriction enzymes and ligated with the plasmid. The resulting p2T7-177-PFK construct was linearized with NotI prior to electroporation of $2T1^{T7\text{-}Cas9}$ and *Δfbp.sbp* cell lines in parallel. Clones obtained after phleomycin selection (at 2.5 µg/ml) were tested for a growth defect after tetracycline induction at 1 µg/ml, and validated by qRT-PCR. The ^{Ty}PFK cell line was also created by Cas9 editing in the $2T1^{T7\text{-}Cas9}$ cell line. Following 24 h of Cas9 induction, electroporation was performed with a sgRNA template (primer pair AZ1388 and sgRNA_R), and PURO.^{Ty}PFK cassette (primer pair AZ1281 and AZ1282). Clones were selected with puromycin at 0.1 µg/ml and integration validated by PCR (primer pair AZ1403 and AZ1404) and western blot.

Table 1: Sequences of DNA primers used in the study.

Primer	Sequence	Description
FBPgRNA_F	TAATACGACTCACTATAGGGAGGGTGTGGTGCTTTTCGTGGGGCGTTTTAGAGCTAGAAATAGCAAG	FBP F sgRNA
sgRNA_R	GCACCGACTCGGTGCCACTTTTTCAAGTTGATAACGGACTAGCCTTATTTTAACTTGCTATTTCTAGCTCTAAAAC	R sgRNA universal
FBP.NPT50_5	ttttgcgactgtttttcaatttcattaacgacaccactcttcccagatttATGATTGAACAAGATGGATTGC	FBP.G418 cassette F
FBP.NPT50_3	TTTTAAAAAAAACCTGTACCCTTTCCACACGCATCGAAGCAACCATTGGCTCAGAAGAACTCGTCAAGAAGG	FBP.G418 cassette R
SBPgRNA_F	TAATACGACTCACTATAGGG TGTGGTGCTTTTCGTGGGGCGTTTTAGAGCTAGAAATAGCAAG	SBP F sgRNA
SBP.PAC50_5	gcccgttacaggggttccctttcactcaacctttcgtggaaagggagaatATGACCGAGTACAAGCCC	SBP.puro cassette F
SBP.PAC50_3	gatcggaccatcaccttgtgcggcacaaaaataaaaacaagaagaaaaaaGGTACCGAGCTCGAATTCTC	SBP.puro cassette R
AZ1211	GATGGCGATTCAAACGTCCG	*FBP* ORF 177 – 981 bp
AZ1212	TTATCCCCCGGGTAGCAGAA	*FBP* ORF 177 – 981 bp
AZ1213	ATTGGCTTCTACCGCGCATA	*SBP* ORF 438 – 1,050 bp
AZ1214	GTTCGTCAACCCCGTTGTTG	*SBP* ORF 438 – 1,050 bp
AZ1339	ATGGATCCTTCACTTCAACCCGACGGAG	PFK RNAi F, *PFK* 338 – 894 bp
AZ1340	ATAAGCTTCTGTCACGACCCATGAGCTT	PFK RNAi R, *PFK* 338 – 894 bp
AZ1388	TAATACGACTCACTATAGGGGTGACGAGCTTGCTCGTAACGGTTTTAGAGCTAGAAATAGCAAG	Ty.PFK sgRNA
AZ1281	GTGAACTGGAGGCAATCAACAGGAATCGCGACCGCCTCCACGAGGAACTGGAGGTCCATACTAACCAAGATCCACTTGACGCCAAGCTCTAATCTCCGCTCTTATTTAGTTTTGC	PURO.^{Ty}PFK cassette F
AZ1282	GTGCCCTCCTCATTCTCCCTTTCCCAGAACTCCGTTACCAGAGGGTCATTCAATCATGTCGACACACCAAG	PURO.^{Ty}PFK cassette R
AZ1403	GGACGTATTGCATGTGCTGTC	validation of ^{Ty}PFK F
AZ1404	TGAGTCACGCTGTTCAGCAT	validation of ^{Ty}PFK R
AZ1550	TAATACGACTCACTATAGGGCGCTACACTTTTGTAAGGGAGTTTTAGAGCTAGAAATAGCAAG	TAL sgRNA
AZ1551	CTTAGAAGGGGGAAGGCAACAAGACATGGCCAAGTTGACCAGTG	TAL phleo cassette F
AZ1552	GTTACTTGATGGTGGGTACCCTCCCTCAGTCCTGCTCCTCGG	Tal phleo cassette R
AZ1609	ATGGATCCGTCTCTCGGCTACGTGATGG	validation of Δ*tal*
AZ1610	ATAAGCTTTCGTTACAGCAATGACGCCT	validation of Δ*tal*

qRT-PCR

Total RNA was extracted from 1 – 2 x 10^8 cells using the RNeasy kit (Qiagen). DNA was removed by Turbo DNase (Applichem) at 37° C for 30 min, which was subsequently treated with DNase inactivation reagent (Ambion) for 5 min at RT. Following ethanol precipitation, cDNA was synthesised from 2 µg of RNA using TaqMan Reverse Transcription Reagent (Applied Biosystems) and random hexamer primers. Real-time PCR amplification was performed using LightCycler 480 SYBR Green I Master (Roche) and LightCycler 480 thermocycler (Roche). Primers used for the PFK target and reference genes are listed in Table 2.

Table 2: Sequences of DNA primers used for qRT-PCR.

Target gene	Primer name	Sequence
PFK F	AZ1489	CCTCACGGAGAAAGTGAAGG
PFK R	AZ1490	GGGTAGCGAGACTTGTTTGC
18S F	AZ50	GCGAAACGCCAAGCTAATAC
18S R	AZ51	AGCCGCGACATAGAAAAAGA
Tubulin F	AZ52	GCAGAGTCCAACATGAACGA
Tubulin R	AZ53	CGTCCGCGTCTAGTATTGCT

Subcellular fractionation and western blotting

In order to separate organellar fractions containing glycosomes from the cytosol, cells were subjected to digitonin-based subcellular fractionation and the obtained samples used for western blots. Briefly, 1 x 10^8 cells were harvested, washed in 1 x PBS and resuspended in 500 µl of SoTE buffer (0.6 M sorbitol, 2 mM EDTA, 20 mM Tris-HCl, pH 7.5). A further 500 µl of SoTE buffer containing 0.03 % digitonin (Sigma-Aldrich) was added, samples were incubated on ice for 5 min and subsequently centrifuged at 4,500 g, 4° C for 3 min. The obtained supernatant was used as cytosolic fraction, and pellets resuspended in equivalent volume of 1 x PBS and used as organellar fractions. 40 µl of samples were loaded for western blots.

For whole cell lysates, the equivalent of 1 x 10^7 cells was used. For western blots (WB) 4-12 % NuPAGE polyacrylamide gels (Invitrogen) and 1 x SDS running buffer (25 mM Tris, 192

mM glycine, 1 % SDS) were used. Subsequently, proteins were transferred to a PVDF membrane (Pierce) in transfer buffer (39 mM glycine, 48 mM Tris, 20 % methanol) at 90 V for 90 min at 4 °C. Following 30 min blocking in 5 % milk (Serva) in PBS-Tween (0.05 %), primary antibody was incubated in milk solution overnight at 4 °C. Following 3 x 10 min wash in PBS-Tween, secondary antibody was incubated in milk solution for 1 h at RT. Following 3 x wash in PBS-T, signal was visualised by Western ECL Substrate (BioRad). The following antibodies were used: α-FBP at 1:500 , α-SBP at 1:500 (both kind gifts from Frederick Bringaud), anti-Ty 1:1,000 (ThermoFisher), α-APRT at 1:500 was used as a marker for cytosolic fraction, and α-hexokinase at 1:2,000 as an organellar marker. Secondary α-mouse (BioRad) and α-rabbit (BioRad) antibodies conjugated to HRP were used at 1:2,000.

Metabolomics

For the experiment with *Δfbp.sbp* in ^{13}C-glycerol, cells were grown in the standard HMI-11 medium supplemented with 5 mM ^{13}C-U-glycerol (Cambridge Isotope Laboratories). For the experiment with *Δfbp.sbp*/^{RNAi}PFK, Δ*tal*, and Δ*fbp.sbp.tal*, HMI-11 medium was prepared from components according to the recipe (Hirumi), but glucose was completely omitted and instead 5 mM $^{13}C_3$-U-glycerol (Cambridge Isotope Laboratories) was supplied. Cells were grown in this medium for 24 h (PFK cell lines) or 48 h (TAL cell lines) prior to sample extraction.

Samples for the metabolomic experiments were prepared by the same extraction protocol as reported previously (Creek). Briefly, 5 x 10^7 cells were used per each 100 µl sample, which were first rapidly cooled to 4° C in a dry ice – ethanol bath. Following a wash with 1 x PBS, the cell pellet was resuspended in 100 µl of chloroform:methanol:water (1:3:1) suspension and incubated with shaking at 4° C for 1 h in order to achieve full extraction into the solvent. Subsequently, samples were centrifuged (12,000 g, 10 min, 4° C), supernatants were collected and stored at -80° C until analysis.

The analysis was performed using separation on 150 x 4.6 mm ZIC-pHILIC (Merck) on a Dionex UltiMate 3000 RSLC system (Thermo Scientific) followed by mass detection on Orbitrap QExactive (Thermo Fisher Scientific) mass spectrometer (Thermo Fisher) at Glasgow Polyomics. Analysis was operated in polarity switching mode, using 10 µl injection volume and a flow rate of 300 µl/min. The analyses was performed in 4 replicates, and a set of standards was run in parallel. Metabolite identification was based on matches with standards where possible or else predicted based on mass and retention time. Data were analysed using mzMatch [29] and mzMatch.ISO [30].

FBPase assay

2 x 10^7 cells were used per sample. They were centrifuged (1,300 g, 10 min), washed with 1 x PBS and resuspended in 100 µl of SoTE buffer (10 mM Tris-HCl pH 8, 1 mM EDTA, 0.15 % Triton X-100, protease inhibitor cocktail (Roche)). After 20 min incubation at RT, samples were centrifuged (14,000 g, 10 min, 16° C) and supernatant collected. The reaction mixture containing 20 mM Tris pH 7.8, 10 mM $MgCl_2$, 1 mM NADP, 1 U PGI (Sigma-Aldrich), 1 U G6PDH, 100 µl cell extract was incubated at 30° C for 5 min prior to activity measurement. The reaction was triggered by addition of 5 mM F1,6bP (Sigma-Aldrich) immediately prior to measurement of NADPH production at 340 nm for 5 min at 30° C using a UV-1601 spectrophotometer (Shimadzu).

IFA

For the immunofluorescence assay, cells were fixed in 7.4 % formaldehyde in 1 x PBS for 15 min, and subsequently washed 3 x with 1 x PBS. For permeabilisation, 0.1 % Triton X-100 (AppliChem) in 1 x PBS was applied for 10 min, and subsequently washed 3 x with 1 x PBS. Following blocking in 5.5 % FBS in 1 x PBS-Tween (0.05 % Tween) and 2 x wash with 1 x PBS, the primary antibodies were applied (α-Ty at 1:100 (ThermoFisher) and α-FBP at 1:1,000) for 1 h at RT. Following three washes with 1 x PBS-T and two washes with 1 x PBS, the secondary antibodies were applied (Alexa Fluor 647 α-mouse (Life Technologies) at 1:2,000 and Alexa Fluor 488 α-rabbit (Life Technologies) at 1:2,000) for 1 h at RT. After an additional three washes with 1 x PBS-T and two washes with PBS, ProLong Gold Antifade mounting solution (Invitrogen) was applied. Imaging was performed using an Axioplan microscope (Zeiss).

Results

Generation of double knock-out *Δfbp.sbp* by two step Cas9 editing

We took advantage of CRISPR/Cas9-based gene editing [27] to generate a double knock-out of FBPase and SBPase (*Δfbp.sbp*) in *T. brucei* BSF. An sgRNA template and a repair template were simultaneously electroporated in a transient transfection, resulting in replacement of both alleles of the *FBPase* gene with a G418 resistance cassette. Subsequently, applying the same approach, both alleles of *SBPase* were replaced with a puromycin cassette (Fig. 1B). Full replacement of all alleles was validated by PCR and western blotting (Fig 1C, D). Such a straightforward replacement of both target genes indicated that FBPase and SBPase most likely do not play essential roles under the growth conditions used. Accordingly, the *Δfbp.sbp* cell line showed no growth defect in the standard nutrient-rich HMI-11 medium (Fig 1E). When Creek's Minimal Medium (CMM), which better approximates the composition of blood serum, was used for cell culture, *Δfbp.sbp* cells suffered a mild growth defect with higher variability, possibly due to different metabolic adaptations required for growth in CMM (Fig 1E) [31]. Because these experiments showed a growth defect under nutrient-restrictive conditions, we decided to assess infectivity *in vivo*. Infection of mice showed that *Δfbp.sbp* cells were infectious, although they reached significantly lower parasitaemia on day 2 compared to the parental cell line (0.6-fold, $p = 0.04$ (Supp Fig 1)).

Figure 1. Generation and growth analysis of Δ*fbp.sbp* strains.

A – The scheme shows glycolysis, gluconeogenesis, and the pentose phosphate pathway in BSF *T. brucei* with highlighted FBPase, PFK, and TAL. Missing reactions of transketolase are depicted by grey arrows.

B – A scheme for the Cas9 editing method by transient transfection. The templates for sgRNA and for the antibiotic resistance cassette were transfected simultaneously, which resulted in replacement of both alleles for *FBPase* in the first step, and for *SBPase* in the second step.

C – Validation of the Δ*fbp.sbp* cell line by PCR, shows parts of ORFs for *FBPase* and *SBPase* amplified in the parental $2T1^{T7.Cas9}$ cell line, but absent from Δ*fbp.sbp*.

D - Validation of the Δ*fbp.sbp* cell line by western blotting. Only the parental cell line shows signal for FBPase (whole cell lysates) and SBPase (organellar fractions), * - cross-reacting protein, gel loading – fluorescent protein detection on a TGX gel.

E – Growth curves of two independent clones of Δ*fbp.sbp* show no defect in the standard HMI-11 medium. Growth curves in the CMM medium show a mild growth defect of the Δ*fbp.sbp* clones and higher variability.

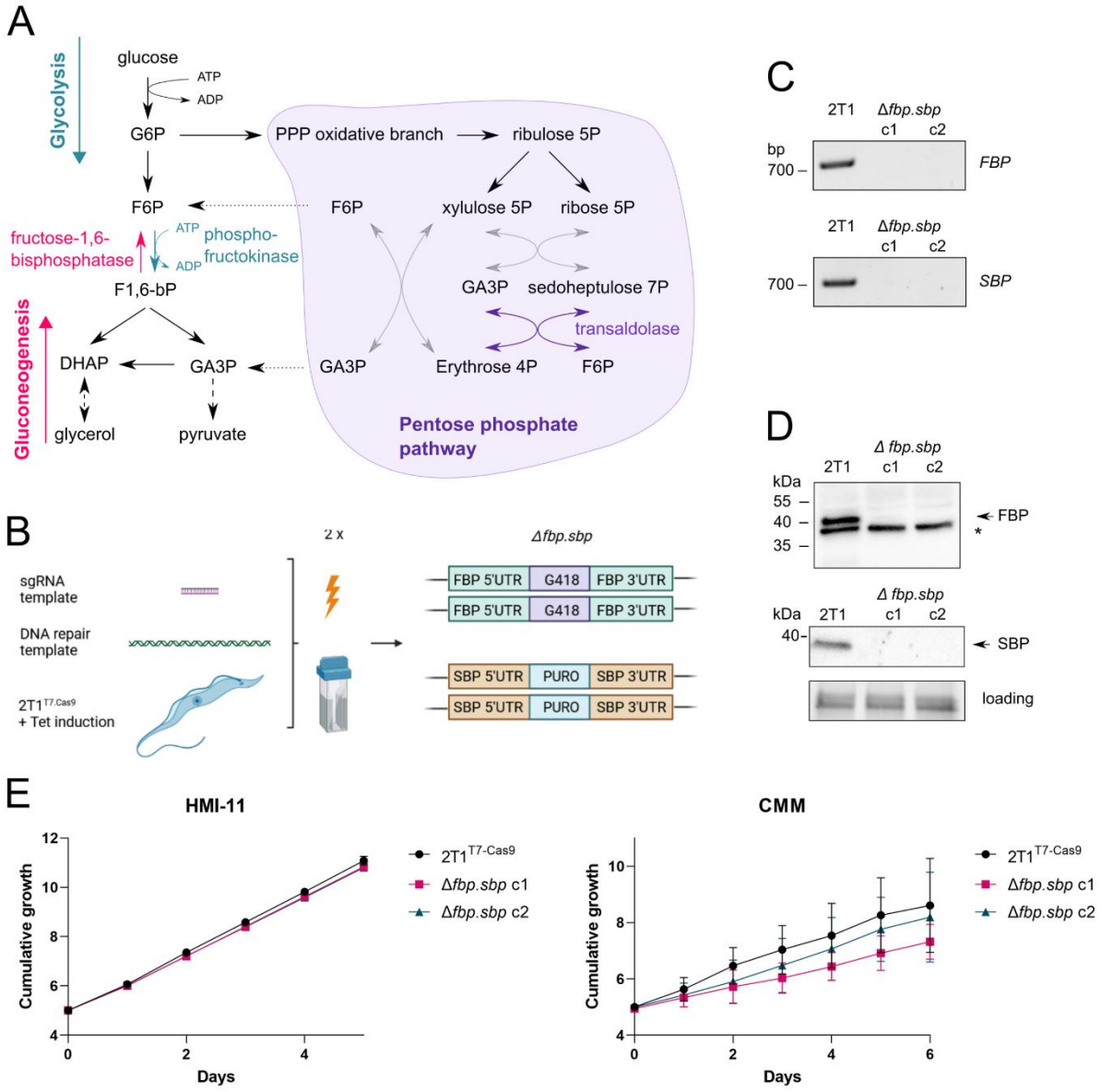

Metabolomic analysis of *Δfbp.sbp* shows sugar phosphate substrate accumulation and maintained gluconeogenesis

We next examined the effects of the double gene deletion on carbon metabolism. First, a metabolomic analysis was performed on *Δfbp.sbp* cells cultured in CMM. The most striking change was approx. 30-fold accumulation of S1,7bP, the substrate of SBPase, (Fig 2A,B), confirming disruption of the SBPase reaction. Sedoheptulose 7-phosphate (S7P) was 4-fold increased, probably due to non-enzymatic conversion of highly accumulated S1,7bP. The

metabolites of the FBPase reaction were also affected, although to a much lesser extent than for SBPase, with F6P increased 1.3-fold, and F1,6bP not changed significantly (Fig 2B). Since F6P and F1,6bP are also involved in other metabolic pathways, especially glycolysis, absence of FBPase does not have such a substantial impact on their abundance.

To test whether GNG flux is present, we grew the parental and *Δfbp.sbp* cells in HMI-11 medium supplemented with 5 mM U-$^{13}C_3$-glycerol and subjected the samples to metabolomic analysis. Overall, only a few changes in the metabolome were observed, with 2-fold accumulation of S7P being most evident in *Δfbp.sbp* cells grown with glycerol (Fig 2C). Since glucose was also present in the medium, the predominant portion of the hexose phosphate isotopomer pool was unlabelled in both cell lines, however, $^{13}C_3$ labelling represented 10 % of the hexose phosphate pool. 12 % of F1,6bP contained the $^{13}C_3$ label, providing a clear evidence that these labelled carbons originate from U-$^{13}C_3$-glycerol fed through GNG, in both parental and *Δfbp.sbp* cell lines (Fig 2C).

Changes in metabolites in CMM (Fig 2B) correspond with the growth defect observed in that medium and reflect higher sensitivity of cells to perturbations in nutrient-restricted conditions, in contrast to the HMI-11 medium, where minimal changes in the metabolome and no growth defect were observed. Overall, the differences detected in sugar phosphates correlate with expectations for FBPase and SBPase deletion, except for gluconeogenic flux being maintained. That was also confirmed when assaying the conversion of F1,6bP to F6P. Comparable levels were measured using a specific enzyme activity assay with cell extracts obtained from the parental cell line (15 µmol/min/mg, n = 3) and *Δfbp.sbp* (16 µmol/min/mg, n = 3).

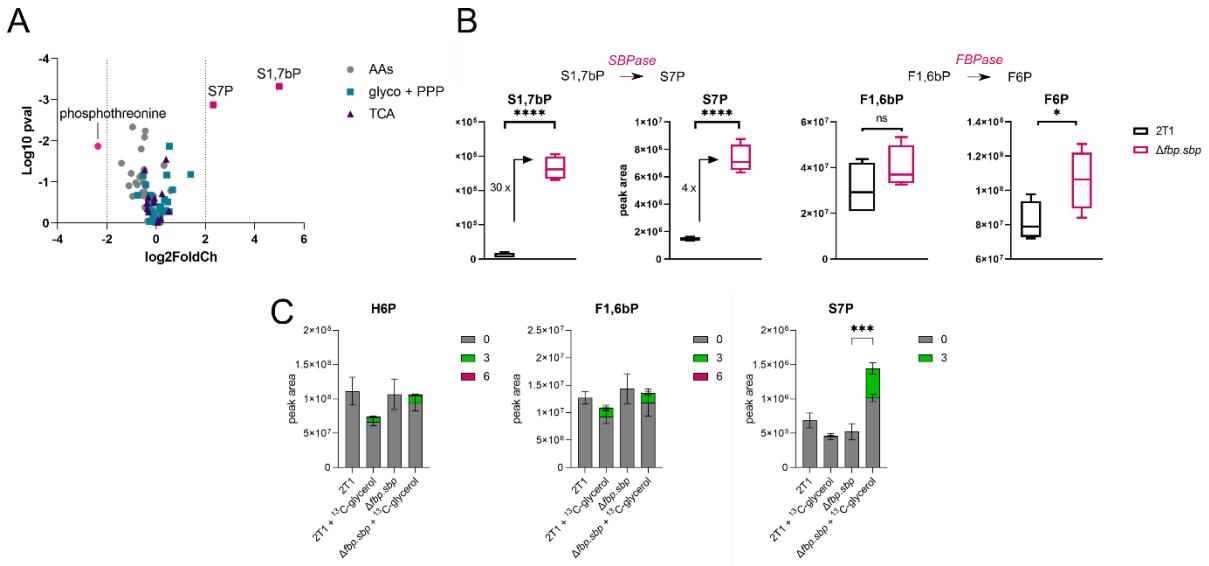

Figure 2. Gluconeogenic activity is maintained in Δ*fbp.sbp* strains.

A – Changes in Δ*fbp.sbp* cells grown in CMM and subjected to non-targeted LC-MS metabolomics when compared to the parental cell line. The most changed metabolites are S7P, S1,7bP, and phosphothreonine. The plot includes 87 metabolites from glycolysis, PPP, TCA cycle or amino acid metabolism.

B – Sedoheptulose 1,7-bisphosphate (S1,7bP), sedoheptulose 7-phosphate (S7P), fructose 6-phosphate (F6P) as detected in the parental and Δ*fbp.sbp* cells grown in CMM and subjected to non-targeted LC-MS metabolomics.

C - Δ*fbp.sbp* cells were grown in HMI-11 supplemented with U-$^{13}C_3$-glycerol and analysed by LC-MS metabolomics, showing that ^{13}C from glycerol is incorporated into GNG products. H6P – hexose 6-phosphates.

<u>Depletion of PFK reduces glycolysis but not GNG</u>

Since we did not observe changes in the GNG flux in *Δfbp.sbp* cell lines, we decided to test if the reversed activity of PFK (dephosphorylation of F1,6bP into F6P) can contribute to GNG. PFK was depleted by RNA interference in the parental cell line (PFK^{RNAi}) and in the *Δfbp.sbp* background (*Δfbp.sbp*/PFK^{RNAi}). Induction of knockdown using tetracycline caused a severe growth defect in both cell lines, as expected, and due to the essential role of PFK in glycolysis (Fig 3A). RT-PCR confirmed a drop in expression of the target gene, to 20 % in the parental background and 60 % in the *Δfbp.sbp* background (insets, Fig 3A). To test for the GNG activity, we performed a metabolomic analysis of the PFK^{RNAi} and *Δfbp.sbp*/PFK^{RNAi} cells fed with U-

$^{13}C_3$-glycerol as the sole carbon source (no glucose was present in the HMI-11 medium, except for ~0.5 mM glucose from 10 % FBS). Samples were harvested 24 h after tetracycline induction in the glycerol medium and subjected to LC-MS metabolomics. The profile of glycerol 3-phosphate (G3P) serves as a proof that glycerol was taken up and incorporated, since $^{13}C_3$-labelled part represents around 80 % (78 - 85 %) of the total in all sample groups (Fig 3B). Crucially, these cells still utilised glycerol via GNG and incorporated it into hexose phosphate sugars. The profile of F6P shows that the majority (44 – 66 %) is $^{13}C_6$-fructose 6-phosphate, made from $^{13}C_3$-glycerol, in all samples (Fig 3B). The major difference after PFK depletion is in the unlabelled part that originates from glucose via glycolysis including PFK. This fraction decreased from 18 to 8 % of the total amount in PFK^{RNAi} induced samples, confirming a reduction in PFK glycolytic activity. On the other hand, the proportion of the $^{13}C_6$-labelled part increases from 44 to 66 % of the total, showing glycerol incorporation is not diminished. A substantial part of F6P is $^{13}C_3$-labelled (26 – 38 %), indicating that both reactions, phosphorylation of F6P into F1,6P and the reverse dephosphorylation, take place. The same analysis of the F1,6bP profile shows an even higher proportion of $^{13}C_6$-labelled, representing 64 – 74 % across the samples. Smaller changes occur after induction of PFK knockdown, but the same trend as in F6P is observed. The unlabelled part dropped from 6.5 to 2.5 %, $^{13}C_3$ decreased from 29 to 22 %, and $^{13}C_6$ increased from 65 to 75 % (Fig 3B). In the *Δfbp.sbp*/^{RNAi}PFK cell line, no significant changes were detected after knockdown, suggesting that any further perturbation of metabolic flux is lethal for these cells.

Pentose phosphate pathway (PPP) intermediates are labelled to a lesser extent than the hexose phosphates. Around 70 % of the total pentose phosphate pool is unlabelled, while $^{13}C_5$ represents between 11 to 18 %, and $^{13}C_3$ about 5 % (Fig 3C). Octulose 8-phosphate (O8P) has been proposed to be synthesized by transfer of a 3-carbom unit from F6P to R5P and its labelling pattern corresponds to this ($^{13}C_3$ represents ~ 65 %, Fig 3C). S7P, another intermediate of the non-oxidative PPP is substantially labelled. The $^{13}C_3$ part comprised around 20 % of total S7P in the wild-type control and PFK^{RNAi}, and 28 % in *Δfbp.sbp*/^{RNAi}PFK, regardless of whether knockdown was induced or not, suggesting that PFK depletion has little impact on the incorporation of glycerol. However, depletion of FBPase and SBPase caused increase in $^{13}C_3$, in addition to the increase in total amount more than 4-fold (compared to WT) (Fig 3C), consistent with the previous measurement (Fig 2B). Moreover, the $^{13}C_7$ part represented about 30 % of total S7P in *Δfbp.sbp* cells, validating glycerol as a substrate for the production of S7P. These larger sugar phosphates have been observed in *T. brucei* before [32], and although their

role in metabolism remains unclear, this targeted metabolomic data offers new insights into their biosynthesis.

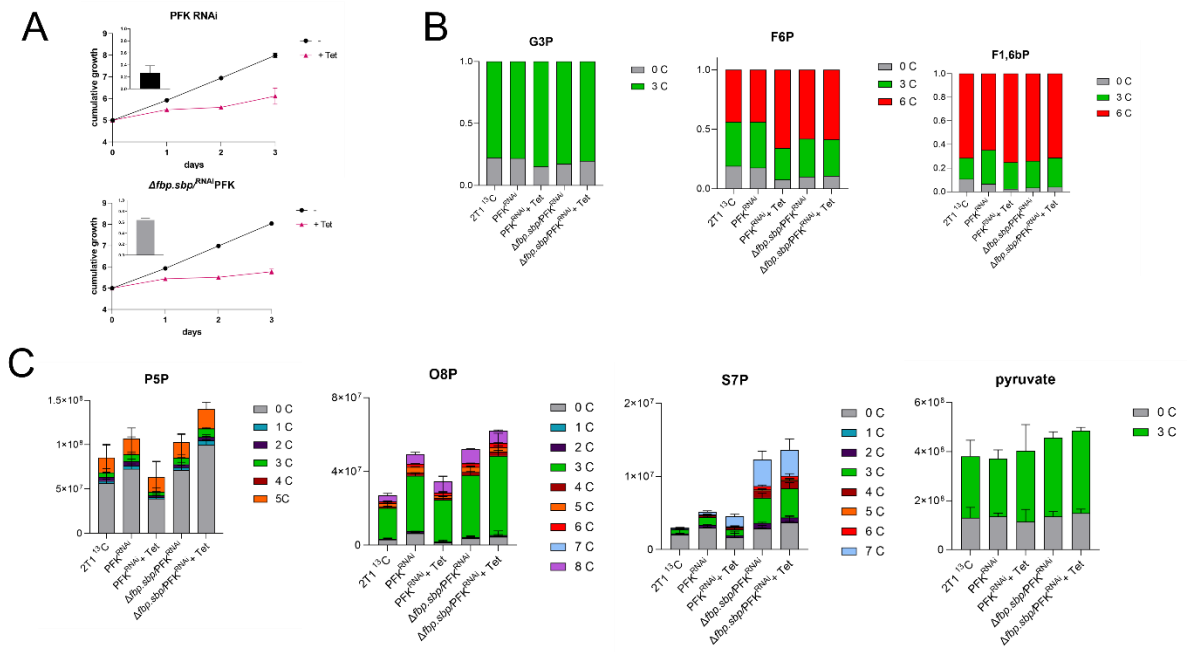

Figure 3. PFK knockdown causes a severe growth defect, but only mild changes in the metabolome.

A – Growth curves of PFK^{RNAi} and in *Δfbp.sbp*/^{RNAi}PFK show a severe growth defect after RNAi induction by tetracycline. Levels of PFK mRNA are shown as detected by qRT-PCR, compared to non-induced cells, and normalised to 18S non-induced, 24 h tetracycline induction (insets).

B – Targeted LC-MS metabolomics in HMI-11 medium depleted of glucose, but supplemented with $^{13}C_3$-glycerol. The proportion of the C_{13} label incorporation relative to the total amount is indicated. G3P – glycerol 3-phosphate, F6P – fructose 6-phosphate, F1,6bP – fructose 1,6-bisphosphate. 2T1 ^{13}C – parental cell line in medium with ^{13}C-glycerol,

PFK^{RNAi} – non-induced PFK RNAi cell lines in medium with ^{13}C-glycerol,

PFK^{RNAi} + Tet – PFK RNAi induced for 24 h in medium with ^{13}C-glycerol,

Δfbp.sbp/PFK – non-induced *Δfbp.sbp*/^{RNAi}PFK cell line in medium with ^{13}C-glycerol, *Δfbp.sbp*/PFK + Tet - *Δfbp.sbp*/^{RNAi}PFK cell line induced for 24 h in medium with ^{13}C-glycerol

C – Same as in B), but the total levels of metabolites are depicted. P5P – pentose 5-phosphates, O8P – octulose 8-phosphate, S7P – sedoheptulose 7-phosphate.

Metabolomic profiles of other metabolites, such as intermediates of glycolysis, the succinate shunt or mitochondrial carbon metabolism provide additional valuable information about the overall metabolism. Substantial $^{13}C_3$ labelling was also observed in phosphoenolpyruvate (PEP), pyruvate, fumarate, malate, aspartate, or alanine (Fig 3C, Supp Fig 2). 72 – 78 % of PEP is $^{13}C_3$, demonstrating a high level of utilisation of labelled glycerol in glycolysis. The unlabelled fraction dropped from 22 % to 13 % after PFK knockdown, again confirming a drop in glucose utilisation in glycolysis, relative to glycerol. Total pyruvate comprises around 30 % (28 – 36 %) of unlabelled, and 60 – 68 % of $^{13}C_3$-pyruvate. Of malate, between 43 % to 57 % is unlabelled, 10 – 16 % is $^{13}C_2$ (synthesized in the mitochondrion via acetyl-CoA), and 28 % - 36 % is $^{13}C_3$ (synthesized in the glycosomal succinate shunt), without significant differences between the sample groups (Supp Fig 2). For aspartate, the $^{13}C_3$ content ranges from 42 and 50 % in all cell samples. These data indicate that glycerol is used in glycolysis for pyruvate and acetyl-CoA production and further fed into reactions of the mitochondrial enzymes classically associated with the TCA cycle (Supp Fig 2). The data are consistent with our previous work, where we observed similar labelling patterns with glycerol, indicating an increase in mitochondrial metabolism when cells rely on GNG [6]. Overall, few changes were observed after PFK knockdown, despite the severe growth defect. However, we see clear evidence for diminished glycolysis, but not GNG. The data demonstrate that glycerol is utilised as the main carbon source under these conditions, since the majority of glycolytic intermediates are labelled from $^{13}C_3$-glycerol. In addition to use as a substrate for GNG, glycerol is used for synthesis of S7P, which may reflect a novel variation of the non-oxidative PPP.

PFK and FBPase co-localise in glycosomes

We next sought to establish the localisation of the key glycolytic and GNG enzymes, PFK and FBPase. Both of these enzymes are glycosomal, but their mutual co-localisation has never been reported. For this purpose, one of the endogenous PFK alleles was tagged in the 2T1$^{T7\text{-}Cas9}$ cell line with the Ty-tag, generating ^{Ty}PFK, which was used for microscopy in a combination with a specific α-FBPase antibody. We cultured the cells in medium supplemented with glucose or glycerol only, or in a combination of both carbon sources, and then subjected them to super-resolution confocal microscopy (Fig 4). PFK and FBPase always co-localised in glycosomes and no differences were observed under the various conditions tested. The two enzymes are not separated by compartmentalisation, and further work will be required to reveal their potential regulation, although futile cycling does occur to some extent as seen in our metabolomic data (Fig 3B).

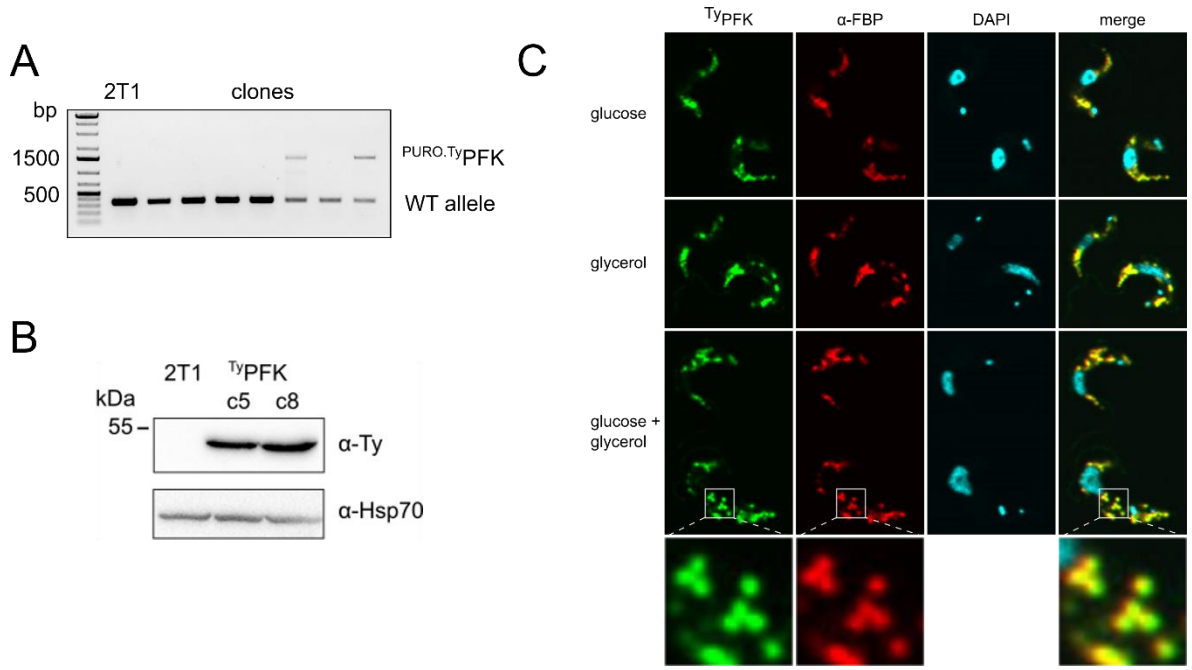

Figure 4. PFK and FBPase co-localise in glycosomes.

A – PCR validation of ^{Ty}PFK clones.

B – Western blot validation of the ^{Ty}PFK cell line.

C – Immunofluorescence assay with ^{Ty}PFK cell line, α-Ty, and α-FBPase staining. Cells were cultured in CMM with different carbon sources (glucose, glycerol, or both), but it had no effect on co-localisation of PFK and FBPase.

<u>TAL does not contribute to gluconeogenesis</u>

A possible explanation for the GNG activity observed (i.e. generation of F6P from glycerol) may be provided by a novel metabolic pathway, as suggested previously [33]. This would include three enzymes (SBPase, TAL, and fructose-1,6-bisphosphate aldolase) working in a cycle, using glycolytic intermediates as substrates to produce F6P (Fig 5A). Considering the unprecedented presence of SBPase, expression of TAL in the absence of transketolase, and the persisting GNG flux in our datasets, this novel pathway would offer a potential solution. Hence, we decided to test the role of TAL in GNG, and generated a knock-out cell line lacking three genes, *FBPase*, *SBPase*, and *TAL* (*Δfbp.sbp.tal*). *TAL* was deleted using Cas9 and replaced with a phleomycin resistance cassette in the parental 2T1$^{T7\text{-}Cas9}$ and in the *Δfbp.sbp* cell lines (Fig 5B). The *Δfbp.sbp.tal* cells showed no growth defect in HMI-11 medium supplemented

either with glucose or glycerol as the main carbon source (Fig 5C). The cells were also still infective to mice at levels comparable to the parental cell line (Supp Fig 3).

A targeted LC-MS metabolomic analysis was performed on cells grown in CMM supplemented with 5 mM $^{13}C_3$-glycerol and no glucose (only 0.5 mM glucose was present due to supplementation with 10 % FCS). The results showed again substantial uptake of, and reliance on, glycerol as the major carbon source. The profile of G6P is surprisingly similar between the parental and *Δfbp.sbp.tal* cells when fed with $^{13}C_3$-glycerol, with the majority of the G6P metabolite being $^{13}C_6$-labelled (62 % in WT and 49 % in *Δfbp.sbp.tal*) (Fig 5D). Even more substantial is the fully labelled part in F1,6bP, representing 84 % of total in WT and 78 % in *Δfbp.sbp.tal*. Additionally, the total amount of the G6P metabolite is 2-fold increased in the triple knock-out (Fig 5D). S7P is a sugar phosphate formed by an unknown mechanism, however, our data show that it is synthesized from glycerol. Its total amount is increased 3-fold in WT when fed on glycerol in contrast to glucose, suggesting that the presence of glycerol supports synthesis of S7P. In addition, it is increased 2-fold in *Δtal* and 6-fold in the *Δfbp.sbp.tal* cell line. The majority is $^{13}C_3$- and $^{13}C_7$-labelled (28 % and 49 % respectively, in *Δfbp.sbp.tal*, Fig 5D). Corresponding to the growth in glycerol medium, the metabolomic data show persistence of GNG flux from glycerol even in the *Δfbp.sbp.tal* cell line. Overall, we did not observe any other major changes in the metabolome associated with deletion of TAL, thus a function for this enzyme in BSF trypanosomes where it is present in the absence of transketolase, its usual partner enzyme within the PPP, remains unknown.

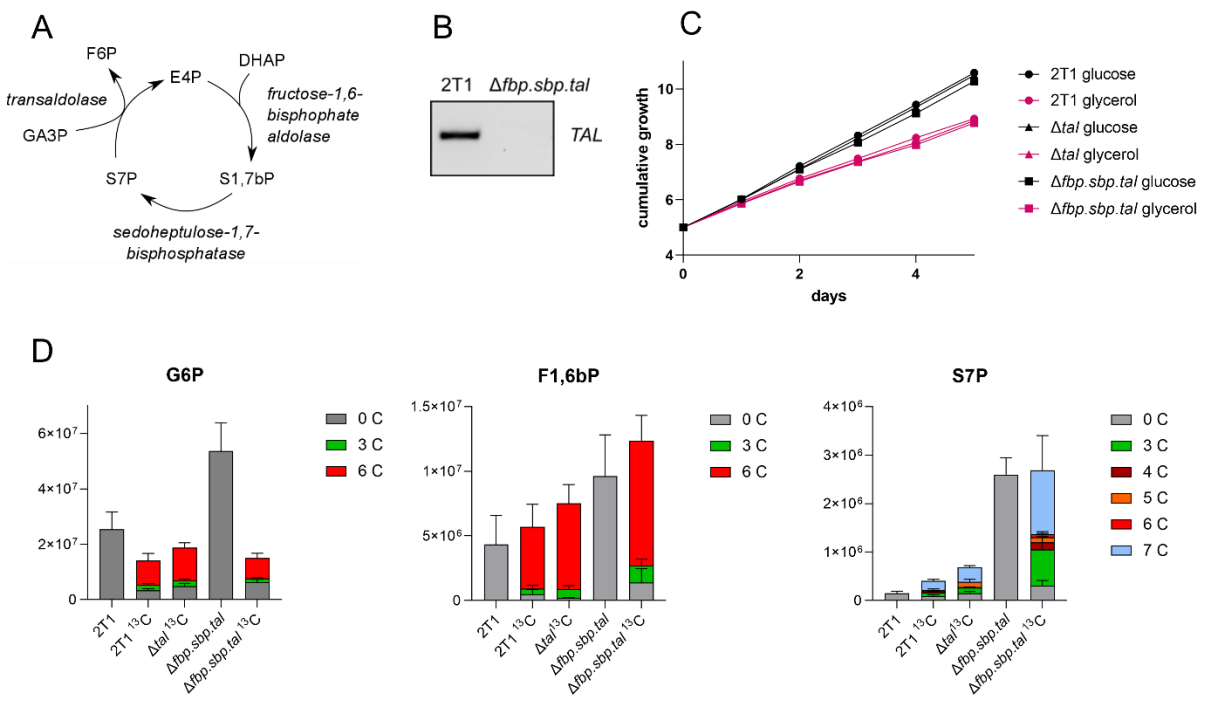

Figure 5. Deletion of TAL does not decrease GNG flux.

A- The novel pathway as suggested by Hannaert [33]: Erythose 4-phosphate (E4P) is condensated with dihydroxyacetone phosphate (DHAP) by fructose-1,6-bisphosphate aldolase into S1,7bP, which is dephosphorylated by SBPase into S7P. That is used as a substrate by transaldolase, together with glyceraldehyde 3-phosphate (GA3P), and converted into F6P and E4P, which can enter another cycle.

B – PCR detection of a 500-bp product from the *TAL* ORF, proving deletion of the gene.

C – Growth curves of the parental (2T1$^{T7\text{-}Cas9}$), *Δtal,* and *Δfbp.sbp.tal* cell lines in HMI-11 medium supplemented with glucose, or glycerol only (and 10 % FBS).

D - Targeted LC-MS metabolomics in CMM supplemented with 5 mM $^{13}C_3$-glycerol. G6P – glucose 6-phosphate, F1,6bP - fructose 1,6-bisphosphate, S7P - sedoheptulose 7-phosphate. 2T1 – parental cell line in medium with glucose, 2T1 ^{13}C – parental cell line in medium with ^{13}C-glycerol, *Δtal*^{13}C – *Δtal* cell line in medium with ^{13}C-glycerol, *Δfbp.sbp.tal* - *Δfbp.sbp.tal* cell line in medium with glucose, *Δfbp.sbp.tal*^{13}C - *Δfbp.sbp.tal* cell line in medium with ^{13}C-glycerol.

Discussion

We took advantage of Cas9-based gene editing to prepare mutants in multiple genes in order to abolish GNG in BSF *T. brucei*. However, our data show that combined deletion of FBPase, SBPase, and TAL had little impact on gluconeogenic activity. To the best of our knowledge, this is the first case of deletion of three gene loci simultaneously in BSF *T. brucei*. Depletion of PFK was possible only to a limited extent, but our data do not indicate that the enzyme is involved in GNG, as suggested previously [18]. Current understanding of trypanosome metabolism does not provide an alternative explanation for how GNG operates, and which other enzymes could contribute to GNG flux.

In our previous work and work of others, it was demonstrated that deletion of the canonical *FBPase* gene in *T. brucei* does not deplete FBPase activity, i. e. conversion of F1,6bP to F6P [6, 7]. This is in contrast to closely related leishmania parasites, where *FBPase* deletion disrupted GNG and caused a severe phenotype in mammalian infective amastigotes [34]. Since SBPase is not present in the genome of leishmania, this enzyme was a promising candidate for the observed FBPase activity. The enzyme has 26 % sequence identity to FBPase, and its catalytic activity is predicted to be very similar, only using a sugar phosphate backbone extended by one carbon. Additionally, SBPase from yeast was demonstrated to posess 'FBPase' activity [35]. The origin of SBPase in trypanosomes remains unclear, but the most probable origin is acquisition by a horizontal gene transfer [36].

The streamlined protocol for Cas9-based gene editing allowed us to generate a double gene knock-out combined with a knock-down. Knock-out for both *FBPase* and *SBPase* genes were easily obtained by single transfections. The *Δfbp.sbp* cell line had no growth defect under nutrient-rich culture conditions. However, there was a mild and variable growth defect in CMM. The high variability in the growth could be caused by different mechanisms of adaptation to nutrient-restricted conditions. The metabolomic experiments with *Δfbp.sbp* revealed that SBPase bears its canonical enzymatic activity (converting S1,7bP to S7P), since its substrate, S1,7bP was highly accumulated in the knockout cell line. A concomitant increase in S7P is most likely explained by non-enzymatic loss of a single phosphate from the accumulated S1,7bP. Similarly, accumulation of S1P and S1,7bP in an SBPase yeast deletion mutant was observed previously [37]. SBPase was also identified in *Toxoplasma gondii*, and its deletion resulted in a similar phenotype to that we observed here, both in metabolomics and in decreased infectivity [38].

Fernandes and colleagues [18] showed reverse PFK activity (equal to canonical FBPase) *in vitro*. In contrast, our data do not support reverse activity of trypanosome PFK *in vivo*, since we observed a decrease in glycolytic flux but not GNG flux. It has been reported previously that PFK is more difficult to knock down than other glycolytic genes [9]. In our knockdown cell lines, we see a very severe growth defect and the PFK mRNA is depleted to 20 % in parental and to 60 % in the *Δfbp.sbp* background. A stronger depletion is probably not possible in the double knock-out, because although metabolic flux is flexible and the enzymes can compensate for each other to some extent, not after multiple deletions. Metabolomics showed surprisingly few changes in the PFK knockdown cell lines. Nevertheless, we detected a decrease in glycolytic flux, but not in GNG flux. The directionality of the PFK activity is dependent on concentrations of substrates and products. Fernandes et al. calculated that the reversal should occur if the concentration of substrates is 500-fold higher than the concentration of products [18]. Changes in ADP, ATP, F6P, and F1,6bP in our metabolomic datasets were much less prominent, for instance one of the greatest changes is 2-fold accumulation of F1,6bP in *Δfbp.sbp*/^{RNAi}PFK compared to wild-type (Supp Fig 3). However, we measure the total cellular metabolite levels, while the ADP/ATP ratio inside glycosomes may be substantially shifted relative to that of the whole cell.

The PPP intermediates detected by metabolomics can be separated into two groups. The first represents the oxidative PPP and metabolites coming originally from glucose, where less labelling from glycerol was detected (pentose phosphates, Fig 3C). The second group, representing the non-oxidative PPP, contains S7P or O8P, which have significant proportions labelled (Fig 3C, 5D). Since BSF *T. brucei* does not express transketolase [21, 22] , the metabolites cannot be produced in the canonical non-oxidative PPP. This suggests that in a low concentration of glucose, as used here, glucose is used preferentially to feed the oxidative PPP, whereas glycerol is used to feed glycolysis and to synthesize these large sugar phosphates S7P and O8P.

A novel metabolic pathway that includes the activities of SBPase, TAL, and fructose-1,6-bisphosphate aldolase was proposed [33]. If active, this pathway conforms to the labelling patterns detected in S7P (and O8P), and also with S1,7bP production catalysed by aldolase, as reported previously [37]. Most importantly, this would present an alternative pathway for the production of F6P from glycerol. Nevertheless, our experiments with the Δ*tal* and Δ*fbp.sbp.tal* mutants show that carbons form glycerol are still incorporated into F1,6bP, F6P, and other

metabolites, demonstrating continued flux though GNG, and precluding the existence of this pathway.

It is also unclear how the flux between glycolysis and GNG, i.e. between PFK and FBPase activity, is regulated. Potentially, the forward or reverse flux could be controlled in some way by the upstream kinases, i.e. hexokinase in glycolysis and glycerol kinase in GNG, as a result of their competition for ATP, as reported recently [12]. Another possibility would be an exclusive compartmentalisation of these enzymes, but our immunofluorescence analysis shows that PFK and FBPase co-localise under all conditions tested. Our work here suggests that some futile cycling does take place, as substantial $^{13}C_3$-labelling of hexose phosphates (Fig 3B) occurs. However, since FBPase is not the main GNG enzyme, we suggest that regulation is achieved by a distinct enzyme that posesses FBPase activity but whose identity is yet to be established.

When glucose is limiting, bloodstream form trypanosomes adapt by activating alternative metabolic pathways. Labelling patterns in succinate and citrate indicate flux in mitochondrial metabolism. Since only a small proportion of labelling in citrate was detected (72 – 89 % of citrate was unlabelled), incorporation of additional substrates, such as glutamine or other amino acids, so far reported as carbon sources only in PCF, but not BSF, likely occurs. Interestingly, production of lactate was detected, labelled from $^{13}C_3$-glycerol, demonstrating its origin from glycolysis. Lactate can be produced from pyruvate in order to maintain the NAD^+/NADH balance as shown in PCF *T. brucei* [39] and this is likely the activity we observe here in BSF.

Deletion and/or depletion of four different genes was not capable of substantially diminishing GNG flux in bloodstream form trypanosomes. Since PFK expression was depleted, we cannot exclude that in the *Δfbp.sbp*/^{RNAi}PFK mutant, the GNG activity is sustained by residual PFK expression. It seems that if glycerol is available to trypanosomes, it is used as a carbon source. Considering the high number of hypothetical proteins in the *T. brucei* genome, another enzyme may be responsible for the activity, currently unrecognized by *in silico* searchers. The question as to whether GNG is essential for BSF *T. brucei* cannot be readily addresses until the key enzyme(s) are identified.

Acknowledgements

We thank Prof. Frederic Bringaud (University of Bordeaux) and Prof. Paul Michels (University of Edinburgh) for a kind gift of antibodies α-FBPase, α-SBPase, and α-PFK. This work was supported by CZ.02.2.69/0.0/0.0/19_074/0016248 LeishWeb to J.K.; by the European Regional Development Fund (ERDF) and Ministry of Education, Youth and Sport (MEYS) project CZ.02.1.01/0.0/0.0/16_019/0000759, by the European Research Council (ERC) under the European Union's Horizon 2020 Research and Innovation Program (MitoSignal, grant agreement no. 101044951), and GACR 20-14409S to A.Z.; D. H. was funded by the Investigator Award from Wellcome Trust [217105/Z/19/Z]. M.P.B was funded by an MRC Newton grant 'Bridging epigenetics, metabolism and cell cycle in pathogenic trypanosomatids' MR/S019650/1.

References

[1] N. P. Crilly and M. R. Mugnier, "Thinking outside the blood: Perspectives on tissue-resident Trypanosoma brucei," (in eng), *PLoS Pathog,* vol. 17, no. 9, p. e1009866, Sep 2021, doi: 10.1371/journal.ppat.1009866.

[2] G. Caljon, N. Van Reet, C. De Trez, M. Vermeersch, D. Pérez-Morga, and J. Van Den Abbeele, "The Dermis as a Delivery Site of Trypanosoma brucei for Tsetse Flies," (in eng), *PLoS Pathog,* vol. 12, no. 7, p. e1005744, Jul 2016, doi: 10.1371/journal.ppat.1005744.

[3] P. Capewell *et al.*, "The skin is a significant but overlooked anatomical reservoir for vector-borne African trypanosomes," (in eng), *Elife,* vol. 5, Sep 22 2016, doi: 10.7554/eLife.17716.

[4] S. Trindade *et al.*, "Trypanosoma brucei Parasites Occupy and Functionally Adapt to the Adipose Tissue in Mice," (in eng), *Cell Host Microbe,* vol. 19, no. 6, pp. 837-48, Jun 8 2016, doi: 10.1016/j.chom.2016.05.002.

[5] D. Mabille *et al.*, "Impact of pulmonary African trypanosomes on the immunology and function of the lung," (in eng), *Nat Commun,* vol. 13, no. 1, p. 7083, Nov 18 2022, doi: 10.1038/s41467-022-34757-w.

[6] J. Kovářová, R. Nagar, J. Faria, M. A. J. Ferguson, M. P. Barrett, and D. Horn, "Gluconeogenesis using glycerol as a substrate in bloodstream-form Trypanosoma brucei," (in eng), *PLoS Pathog,* vol. 14, no. 12, p. e1007475, Dec 2018, doi: 10.1371/journal.ppat.1007475.

[7] E. Pineda *et al.*, "Glycerol supports growth of the Trypanosoma brucei bloodstream forms in the absence of glucose: Analysis of metabolic adaptations on glycerol-rich conditions," (in eng), *PLoS Pathog,* vol. 14, no. 11, p. e1007412, Nov 2018, doi: 10.1371/journal.ppat.1007412.

[8] S. Trindade *et al.*, "Slow growing behavior in African trypanosomes during adipose tissue colonization," (in eng), *Nat Commun,* vol. 13, no. 1, p. 7548, Dec 8 2022, doi: 10.1038/s41467-022-34622-w.

[9] M. A. Albert *et al.*, "Experimental and in silico analyses of glycolytic flux control in bloodstream form Trypanosoma brucei," (in eng), *J Biol Chem,* vol. 280, no. 31, pp. 28306-15, Aug 5 2005, doi: 10.1074/jbc.M502403200.

[10] a. M C Scrutton and M. F. Utter, "The Regulation of Glycolysis and Gluconeogenesis in Animal Tissues," *Annual Review of Biochemistry,* vol. 37, no. 1, pp. 249-302, 1968, doi: 10.1146/annurev.bi.37.070168.001341.

[11] M. Wargnies *et al.*, "Gluconeogenesis is essential for trypanosome development in the tsetse fly vector," (in eng), *PLoS Pathog,* vol. 14, no. 12, p. e1007502, Dec 2018, doi: 10.1371/journal.ppat.1007502.

[12] S. Allmann *et al.*, "Glycerol suppresses glucose consumption in trypanosomes through metabolic contest," (in eng), *PLoS Biol,* vol. 19, no. 8, p. e3001359, Aug 2021, doi: 10.1371/journal.pbio.3001359.

[13] C. N. Cronin and K. F. Tipton, "Purification and regulatory properties of phosphofructokinase from Trypanosoma (Trypanozoon) brucei brucei," (in eng), *Biochem J,* vol. 227, no. 1, pp. 113-24, Apr 1 1985, doi: 10.1042/bj2270113.

[14] N. Chevalier, L. Bertrand, M. H. Rider, F. R. Opperdoes, D. J. Rigden, and P. A. Michels, "6-Phosphofructo-2-kinase and fructose-2,6-bisphosphatase in Trypanosomatidae. Molecular characterization, database searches, modelling studies and evolutionary analysis," (in eng), *Febs j,* vol. 272, no. 14, pp. 3542-60, Jul 2005, doi: 10.1111/j.1742-4658.2005.04774.x.

[15] J. D. Sunter, S. Dean, and R. J. Wheeler, "TrypTag.org: from images to discoveries using genome-wide protein localisation in Trypanosoma brucei," (in eng), *Trends Parasitol,* Mar 14 2023, doi: 10.1016/j.pt.2023.02.008.

[16] I. W. McNae, J. Martinez-Oyanedel, J. W. Keillor, P. A. Michels, L. A. Fothergill-Gilmore, and M. D. Walkinshaw, "The crystal structure of ATP-bound phosphofructokinase from Trypanosoma brucei reveals conformational transitions different from those of other phosphofructokinases," (in eng), *J Mol Biol,* vol. 385, no. 5, pp. 1519-33, Feb 6 2009, doi: 10.1016/j.jmb.2008.11.047.

[17] I. W. McNae *et al.*, "Fast acting allosteric phosphofructokinase inhibitors block trypanosome glycolysis and cure acute African trypanosomiasis in mice," (in eng), *Nat Commun,* vol. 12, no. 1, p. 1052, Feb 16 2021, doi: 10.1038/s41467-021-21273-6.

[18] P. M. Fernandes, J. Kinkead, I. W. McNae, F. Bringaud, P. A. M. Michels, and M. D. Walkinshaw, "The kinetic characteristics of human and trypanosomatid phosphofructokinases for the reverse reaction," (in eng), *Biochem J*, vol. 476, no. 2, pp. 179-191, Jan 18 2019, doi: 10.1042/bcj20180635.

[19] E. Hofmann, "The significance of phosphofructokinase to the regulation of carbohydrate metabolism," (in eng), *Rev Physiol Biochem Pharmacol*, vol. 75, pp. 1-68, 1976, doi: 10.1007/BFb0030484.

[20] P. A. M. Michels and M. Gualdrón-López, "Biogenesis and metabolic homeostasis of trypanosomatid glycosomes: New insights and new questions," (in eng), *J Eukaryot Microbiol*, vol. 69, no. 6, p. e12897, Nov 2022, doi: 10.1111/jeu.12897.

[21] S. A. Stoffel *et al.*, "Transketolase in Trypanosoma brucei," (in eng), *Mol Biochem Parasitol*, vol. 179, no. 1, pp. 1-7, Sep 2011, doi: 10.1016/j.molbiopara.2011.04.006.

[22] C. N. Cronín, D. P. Nolan, and H. P. Voorheis, "The enzymes of the classical pentose phosphate pathway display differential activities in procyclic and bloodstream forms of Trypanosoma brucei," (in eng), *FEBS Lett*, vol. 244, no. 1, pp. 26-30, Feb 13 1989, doi: 10.1016/0014-5793(89)81154-8.

[23] M. Gualdrón-López, A. Brennand, L. Avilán, and P. A. Michels, "Translocation of solutes and proteins across the glycosomal membrane of trypanosomes; possibilities and limitations for targeting with trypanocidal drugs," (in eng), *Parasitology*, vol. 140, no. 1, pp. 1-20, Jan 2013, doi: 10.1017/s0031182012001278.

[24] F. Achcar, M. P. Barrett, and R. Breitling, "Explicit consideration of topological and parameter uncertainty gives new insights into a well-established model of glycolysis," (in eng), *Febs j*, vol. 280, no. 18, pp. 4640-51, Sep 2013, doi: 10.1111/febs.12436.

[25] B. M. Bakker, H. V. Westerhoff, and P. A. Michels, "Regulation and control of compartmentalized glycolysis in bloodstream form Trypanosoma brucei," (in eng), *J Bioenerg Biomembr*, vol. 27, no. 5, pp. 513-25, Oct 1995, doi: 10.1007/bf02110191.

[26] H. Hirumi, J. J. Doyle, and K. Hirumi, "Cultivation of bloodstream Trypanosoma brucei," (in eng), *Bull World Health Organ*, vol. 55, no. 2-3, pp. 405-9, 1977.

[27] E. Rico, L. Jeacock, J. Kovářová, and D. Horn, "Inducible high-efficiency CRISPR-Cas9-targeted gene editing and precision base editing in African trypanosomes," (in eng), *Sci Rep*, vol. 8, no. 1, p. 7960, May 21 2018, doi: 10.1038/s41598-018-26303-w.

[28] B. Wickstead, K. Ersfeld, and K. Gull, "Targeting of a tetracycline-inducible expression system to the transcriptionally silent minichromosomes of Trypanosoma brucei," (in eng), *Mol Biochem Parasitol*, vol. 125, no. 1-2, pp. 211-6, Nov-Dec 2002, doi: 10.1016/s0166-6851(02)00238-4.

[29] R. A. Scheltema, A. Jankevics, R. C. Jansen, M. A. Swertz, and R. Breitling, "PeakML/mzMatch: a file format, Java library, R library, and tool-chain for mass spectrometry data analysis," (in eng), *Anal Chem*, vol. 83, no. 7, pp. 2786-93, Apr 1 2011, doi: 10.1021/ac2000994.

[30] A. Chokkathukalam, A. Jankevics, D. J. Creek, F. Achcar, M. P. Barrett, and R. Breitling, "mzMatch-ISO: an R tool for the annotation and relative quantification of isotope-labelled mass spectrometry data," (in eng), *Bioinformatics*, vol. 29, no. 2, pp. 281-3, Jan 15 2013, doi: 10.1093/bioinformatics/bts674.

[31] D. J. Creek, B. Nijagal, D. H. Kim, F. Rojas, K. R. Matthews, and M. P. Barrett, "Metabolomics guides rational development of a simplified cell culture medium for drug screening against Trypanosoma brucei," (in eng), *Antimicrob Agents Chemother*, vol. 57, no. 6, pp. 2768-79, Jun 2013, doi: 10.1128/aac.00044-13.

[32] D. J. Creek *et al.*, "Probing the metabolic network in bloodstream-form Trypanosoma brucei using untargeted metabolomics with stable isotope labelled glucose," (in eng), *PLoS Pathog*, vol. 11, no. 3, p. e1004689, Mar 2015, doi: 10.1371/journal.ppat.1004689.

[33] V. Hannaert, F. Bringaud, F. R. Opperdoes, and P. A. Michels, "Evolution of energy metabolism and its compartmentation in Kinetoplastida," (in eng), *Kinetoplastid Biol Dis*, vol. 2, no. 1, p. 11, Oct 28 2003, doi: 10.1186/1475-9292-2-11.

[34] T. Naderer *et al.*, "Virulence of Leishmania major in macrophages and mice requires the gluconeogenic enzyme fructose-1,6-bisphosphatase," (in eng), *Proc Natl Acad Sci U S A*, vol. 103, no. 14, pp. 5502-7, Apr 4 2006, doi: 10.1073/pnas.0509196103.

[35] E. Kuznetsova *et al.*, "Structure and activity of the metal-independent fructose-1,6-bisphosphatase YK23 from Saccharomyces cerevisiae," (in eng), *J Biol Chem*, vol. 285, no. 27, pp. 21049-59, Jul 2 2010, doi: 10.1074/jbc.M110.118315.

[36] R. Teich, S. Zauner, D. Baurain, H. Brinkmann, and J. Petersen, "Origin and distribution of Calvin cycle fructose and sedoheptulose bisphosphatases in plantae and complex algae: a single secondary origin of complex red plastids and subsequent propagation via tertiary endosymbioses," (in eng), *Protist*, vol. 158, no. 3, pp. 263-76, Jul 2007, doi: 10.1016/j.protis.2006.12.004.

[37] M. F. Clasquin *et al.*, "Riboneogenesis in yeast," (in eng), *Cell*, vol. 145, no. 6, pp. 969-80, Jun 10 2011, doi: 10.1016/j.cell.2011.05.022.

[38] W. J. Olson *et al.*, "Dual metabolomic profiling uncovers Toxoplasma manipulation of the host metabolome and the discovery of a novel parasite metabolic capability," (in eng), *PLoS Pathog*, vol. 16, no. 4, p. e1008432, Apr 2020, doi: 10.1371/journal.ppat.1008432.

[39] O. Villafraz *et al.*, "Procyclic trypanosomes recycle glucose catabolites and TCA cycle intermediates to stimulate growth in the presence of physiological amounts of proline," (in eng), *PLoS Pathog*, vol. 17, no. 3, p. e1009204, Mar 2021, doi: 10.1371/journal.ppat.1009204.